

Information-Driven Phase Transition on Weighted Graphs with Spontaneous Dimensional Sensitivity

V. Dolci¹

¹*Independent Researcher*
(Dated: March 17, 2026)

We study the dynamics of information flow on a weighted graph whose topology evolves according to a spectral curvature measure \mathcal{R} . The model—termed the Unified Informational Framework (FIU, from the Italian *Framework Informazionale Unificato*)—defines \mathcal{R} from the diagonal of the graph Green function, propagates energy between nodes with curvature-dependent dissipation, and creates new long-range links preferentially between high- \mathcal{R} nodes with a rate controlled by a coupling parameter g .

We report three main results. First, the system exhibits a sharp phase transition at a critical coupling $g_c \approx 0.023$ (confirmed with 10 independent runs per coupling value): below g_c , the local information flux rate σ and topological structure formation are anti-correlated; above g_c , they become strongly positively correlated (Pearson $r \approx 0.75$, $p < 10^{-38}$). The transition displays signatures of a continuous (second-order) phase transition, including critical fluctuations and a mean-field onset exponent $\nu \approx 0.54$.

Second, we identify a node-level discrete Poisson relation $\nabla^2 \mathcal{R}(i) = \kappa \sigma_{\text{prev}}(i)$, where $\nabla^2 \mathcal{R}$ is the graph Laplacian of the curvature field and σ_{prev} is the information flux rate at the previous time step. The emergent parameter κ is stable across model parameters (CV = 1.7% across the ordered phase, CV = 2.6% across four independent configurations at fixed system size $N = 256$). A systematic mediator analysis (Test E) reveals that this correlation is almost entirely mediated by the curvature field \mathcal{R} itself, identifying \mathcal{R} as the central self-organizing variable of the dynamics.

Third, and most strikingly, the correlation and the Poisson relation exhibit *spontaneous dimensional sensitivity*: in two-dimensional initial lattices, both signals decay to zero for $N \gtrsim 576$, while in three-dimensional initial lattices they persist to $N \lesssim 1728$ before collapsing at $N \gtrsim 3375$. This dimensional distinction emerges without any dimensional parameter in the dynamical rules. The mechanism of collapse is identified as graph regularization: at large N , the curvature field homogenizes ($\sigma(\nabla^2 \mathcal{R}) \rightarrow 0$) while information flux fluctuations remain finite. We interpret the signal as a topological frustration phenomenon active in a mesoscopic regime, and discuss structural analogies with the topological nature of $2 + 1$ gravity and the local dynamics of $3 + 1$ gravity.

I. INTRODUCTION

The dynamics of evolving networks—in which both the state of nodes and the topology of connections change simultaneously—have become a central topic in complex systems research. Such systems exhibit emergent phenomena that are qualitatively absent in fixed-topology models: self-organization, phase transitions driven by structural feedback, and the spontaneous appearance of geometric order from purely local rules. The present work studies a model in this class in which the driving variable is an information-theoretic quantity: the local flux rate of energy across graph edges.

A recurring theme in the theoretical physics literature is that spacetime geometry—and gravitational dynamics in particular—may itself be an emergent phenomenon of an underlying information-processing substrate. This *emergent gravity* hypothesis serves as our primary motivation, and connects our model to a rich body of theoretical work. Jacobson [1] derived the Einstein equations from the thermodynamics of local Rindler horizons, identifying entropy and temperature as the fundamental quantities. The Ryu–Takayanagi formula [2] relates holographic entanglement entropy to geometric areas, while the ER = EPR conjecture [3, 13] links quantum entanglement with wormhole connectivity. On the discrete side,

Quantum Graphity [4] models the universe as transitioning from a fully connected pre-geometric phase to an ordered lattice phase; Verlinde’s entropic gravity [5] recasts gravitational attraction as an entropic force on holographic screens; and network-based approaches by Bianconi and Rahmede [14] and Trugenberger [15] demonstrate self-organization of network topologies toward regular geometries. We draw on this literature as conceptual context and motivation. Our model is not a derivation of gravity, but a numerical experiment designed to ask: what structural and dynamical phenomena emerge when a graph is driven by curvature-sensitive information flow?

The Unified Informational Framework (FIU, from the Italian *Framework Informazionale Unificato*) is defined by three minimal rules:

1. A spectral curvature measure $\mathcal{R}(i)$, constructed from the diagonal of the graph Green function, characterizes the local spectral inhomogeneity of each node.
2. Energy is propagated between nodes with dissipation controlled by the curvature contrast between neighbors, creating a feedback between information flux and graph geometry.
3. New long-range links (g-links) are created prefer-

entially between nodes of high \mathcal{R} , with a rate proportional to the coupling parameter g .

Our central findings are:

- (i) A sharp phase transition at $g_c \approx 0.023$ separates an *ordered phase* (strong positive structure-flux correlation, $\text{gravC} \approx 0.75$) from a disordered phase (anti-correlated dynamics), with mean-field critical exponent $\nu \approx 0.54$.
- (ii) A discrete Poisson relation $\nabla^2 \mathcal{R}(i) = \kappa \sigma_{\text{prev}}(i)$ holds node-by-node in the ordered phase, with an emergent coupling parameter $\kappa = 67.85 \pm 1.74$ (CV = 2.6%) that is stable across parameter configurations and independent of g in the ordered phase (CV = 1.7%).
- (iii) A mediator analysis (Test E) identifies \mathcal{R} as the central self-organizing variable: the structure-flux correlation is almost entirely mediated through the curvature field, not through the information flux directly.
- (iv) Spontaneous dimensional sensitivity: the ordered phase exists only in a mesoscopic window $N \lesssim 576$ (2D) or $N \lesssim 1728$ (3D), with the dimensional distinction ($N_c^{3D}/N_c^{2D} \approx 5.9$) emerging without any dimensional parameter in the rules.

We discuss structural analogies between these results and known properties of gravity in 2+1 and 3+1 dimensions, while emphasizing that these parallels remain at the level of analogy.

The remainder of this paper is structured as follows. Section II presents the FIU model in detail. Section III describes our correlation tests, including Test D (discrete Poisson relation) and the new Test E (mediator analysis). Section IV reports numerical results across multiple experimental phases, finite-size scaling, 3D simulations, and the collapse mechanism. Section V interprets the findings. Section VI summarizes conclusions and outlines future work.

II. THE FIU MODEL

A. Graph structure and Laplacian

We consider a weighted undirected graph $G = (V, E, w)$ with $N = |V|$ nodes and weighted adjacency matrix $A_{ij} = w_{ij} \geq 0$, where w_{ij} denotes the weight of the edge between nodes i and j (with $w_{ij} = 0$ for absent edges and $w_{ij} = w_{ji}$ by symmetry). The initial topology is a regular $n \times n$ square lattice ($N = n^2$) with unit edge weights, which evolves dynamically over time.

The weighted graph Laplacian is defined as

$$L = D - A, \quad (1)$$

where $D_{ii} = \sum_j w_{ij}$ is the strength (weighted degree) matrix. L is symmetric positive semi-definite with a zero eigenvalue corresponding to the constant eigenvector (for connected graphs).

B. Spectral decomposition and Green function

We perform a partial spectral decomposition of L , computing the $K = 30$ smallest non-trivial eigenvalue-eigenvector pairs $\{\lambda_k, \varphi_k\}_{k=1}^K$ via power iteration with Hotelling deflation [17]. After computing each eigenpair (λ_k, φ_k) , the matrix is deflated as $L \rightarrow L - \lambda_k \varphi_k \varphi_k^T$, projecting out the found eigenvector and exposing the next eigenvalue. Each eigenvector is computed using 150 power iterations on the shifted matrix $\lambda_{\text{max}} I - L_{\text{deflated}}$. An infrared (IR) regulator $m^2 = 1/N$ is introduced to regularize the zero mode.

The diagonal of the scalar propagator (Green function) is

$$G(i, i) = \sum_{k=1}^{N-1} \frac{[\varphi_k(i)]^2}{\lambda_k + m^2}. \quad (2)$$

A reference (flat-space) value is defined as

$$G_{\text{ref}} = \frac{N-1}{N^2 \sum_{k=1}^{N-1} \frac{1}{\lambda_k + m^2}}, \quad (3)$$

which represents the spatially averaged Green function on a graph with uniform spectral density.

C. Curvature measure

The local curvature at node i is defined as

$$\mathcal{R}(i) = \Gamma \left(1 - \frac{G_{\text{ref}}}{G(i, i)} \right), \quad (4)$$

where $\Gamma = 1/\sigma_{\tilde{R}}$ is a normalization constant, with $\tilde{R}(i) = 1 - G_{\text{ref}}/G(i, i)$ the unnormalized curvature and $\sigma_{\tilde{R}}$ its standard deviation over all nodes. This ensures that \mathcal{R} has unit variance over the graph at each time step. Nodes where $G(i, i) > G_{\text{ref}}$ (i.e., where the propagator exceeds its flat-space expectation) have positive curvature; nodes where $G(i, i) < G_{\text{ref}}$ have negative curvature. This measure is inspired by the role of the heat-kernel diagonal in spectral geometry [6] and by the Ollivier-Ricci curvature on graphs [7].

We emphasize that \mathcal{R} is not a Ricci curvature in the differential-geometric sense; it is a *spectral inhomogeneity indicator* that measures how the local propagator deviates from its spatially averaged value. The connection to continuum curvature is indirect: on a Riemannian manifold, the heat-kernel diagonal encodes the scalar curvature only in the sub-leading term of its short-time asymp-

otic expansion, whereas Eq. (4) uses the full Green function with a finite IR regulator. We retain the term ‘‘curvature’’ following established convention in the graph-curvature literature [7, 11, 12], while acknowledging that \mathcal{R} captures spectral geometry rather than Riemannian curvature *per se*. In what follows, \mathcal{R} should be understood as a measure of spectral inhomogeneity that drives the topological dynamics of the model, not as a literal geometric curvature.

D. Energy propagation and link dynamics

Each node i carries an energy $E_i(t) \geq 0$. At each time step the following updates are applied.

a. Energy decay. Edge weights evolve according to

$$w_{ij}(t+1) = w_{ij}(t) \cdot \exp(-\alpha \cdot E_{\text{eff}} \cdot \mathcal{R}_{\text{eff}}), \quad (5)$$

where $\alpha > 0$ is the decay rate, $E_{\text{eff}} = (E_i + E_j)/2$ is the average energy of the two endpoint nodes, and $\mathcal{R}_{\text{eff}} = |\mathcal{R}(i) - \mathcal{R}(j)|/2 + \epsilon$ is an effective curvature contrast between nodes i and j (with $\epsilon = 10^{-6}$ to prevent vanishing decay). This rule implements dissipation that is stronger in regions of high curvature contrast and high energy density.

b. Activation and link formation. A node i may create a new long-range link (g-link) with probability proportional to $\mathcal{R}(i)^\beta$, where $\beta = 0.8$ is an empirical exponent chosen to provide sub-linear preferential attachment (sensitivity to β is discussed in Section V). The target node j is selected from the high- \mathcal{R} region, and the new link is assigned initial weight

$$w_{ij}^{\text{new}} = g \cdot \mathcal{R}_{\text{src}}, \quad (6)$$

where $g > 0$ is the coupling parameter and $\mathcal{R}_{\text{src}} = \mathcal{R}(i)$.

c. Budget constraint. After each update step, nodal energies are renormalized so that the total energy per node remains equal to the budget parameter B :

$$E_i \leftarrow E_i \cdot \frac{B \cdot N}{\sum_j E_j}. \quad (7)$$

The model is parametrized by three key dimensionless numbers: the decay rate α , the energy budget B , and the coupling g .

III. CORRELATION TEST DESIGN

A central methodological concern is circularity: if the information flux rate σ is defined in terms of links, and long-range links (g-links) are created between high- σ nodes, any positive correlation is trivially guaranteed. We adopt five complementary tests designed to avoid this pitfall. Throughout this section, the labels gravC, gravA, gravB denote correlation coefficients from the original analysis pipeline as defined in the equations below.

A. Test C: Delayed information flux rate (primary)

We define the local information flux rate at node i and time t as

$$\sigma_i(t) = - \sum_{j \in \mathcal{N}(i)} \Delta E_{ij}(t) \log \frac{|\Delta E_{ij}(t)| + \epsilon}{E_i(t) + \epsilon}, \quad (8)$$

where $\mathcal{N}(i)$ is the neighborhood of i , ΔE_{ij} is the energy exchanged along edge (i, j) , and ϵ is a small regularizer. We note that σ_i is a Shannon-type information flux measure quantifying the rate of energy redistribution at node i , distinct from the thermodynamic entropy production rate of stochastic thermodynamics [16].

The ‘‘mass’’ of node i is then defined with a temporal delay $\tau = 50$ steps:

$$m_i(t) = \sigma_i(t - \tau). \quad (9)$$

The ordering signal (correlation signal) is the Pearson correlation coefficient between $m_i(t - \tau)$ and the number of long-range links (g-links) incident on node i at time t :

$$\text{gravC}(t) = \text{Pearson}[\sigma_i(t - \tau), \ell_i^{\text{grav}}(t)], \quad (10)$$

where the correlation is computed over all nodes i at each time step and then averaged over a window. (We retain the label gravC from the original analysis pipeline; it denotes the structure-flux correlation coefficient as defined here. Similarly, gravA and gravB below are pipeline labels for correlation coefficients defined in Eqs. (8) and the scalar-field test respectively.) The temporal delay τ ensures that the mass proxy is measured *before* the long-range links it is hypothesized to attract are formed, thereby breaking the direct feedback loop.

B. Test A: Topological event counter

As an independent cross-check, Test A counts topological events (link creation and deletion episodes) in the vicinity of each node and correlates this count with the local \mathcal{R} value (reported as gravA). A negative gravA indicates that topological activity is suppressed in high-curvature regions, consistent with a picture in which the ordered phase ‘‘freezes’’ the local topology.

C. Test B: External scalar field

Test B introduces an external scalar field $\phi(i)$ that propagates on the graph via a discrete wave equation but does not participate in the coupling. The scalar-field energy density $E_\phi(i) = \frac{1}{2}\dot{\phi}(i)^2 + \frac{1}{2}\phi(i)^2$ provides a mass proxy that is genuinely independent of \mathcal{R} .

Across all 36 Phase 1 runs, $\text{gravB} = -0.021 \pm 0.061$, consistent with zero. The scalar field energy shows no correlation with curvature in any regime: gravB remains

flat ($|\text{gravB}| < 0.04$) across the critical region ($g = 0.018$ – 0.028), the τ -scan ($\tau = 0$ – 500), and the null test at $g = 0$. This confirms that the positive gravC correlation is *specific* to the entropy-driven mass proxy σ_i , rather than a generic artifact of the graph dynamics. Test B thus serves as an independent null test, complementing the $g = 0$ null test described in Phase 5.

D. Test D: Discrete Poisson Relation

Motivated by Jacobson’s derivation of the Einstein equation from thermodynamic relations [1], we formulate a node-level test of a discrete Poisson equation. For each node i at each time step, we compute:

- $\nabla^2 \mathcal{R}(i) = \sum_{j \in \mathcal{N}(i)} w_{ij} [\mathcal{R}(j) - \mathcal{R}(i)]$, the (weighted) graph Laplacian of the curvature field;
- $\sigma_{\text{prev}}(i) = \sigma_i(t-1)$, the information flux rate at the previous time step.

We then perform a linear regression over all nodes i :

$$\nabla^2 \mathcal{R}(i) = \kappa \cdot \sigma_{\text{prev}}(i) + b, \quad (11)$$

extracting the slope κ (emergent coupling parameter), the intercept b , and the coefficient of determination R^2 . The Pearson correlation coefficient of this regression is identical to gravC from Test C, establishing Test D as a quantitative reformulation that provides an absolute scale (κ) rather than only a normalized correlation.

The connection to Jacobson’s framework is a structural analogy. In the continuum, the Einstein equation in the non-relativistic Newtonian limit reduces to the Poisson equation $\nabla^2 \phi = 4\pi G \rho$. The discrete Poisson relation (11) has the same form, with \mathcal{R} playing the role of the potential ϕ , σ_{prev} playing the role of the source density ρ , and $\kappa \leftrightarrow 4\pi G$ (or $8\pi G$ in relativistic notation) as the emergent coupling parameter. We emphasize that this is an analogy: the FIU model does not derive gravity, and κ is a mesoscopic parameter of the graph dynamics, not a fundamental constant.

E. Test E: Mediator Analysis

Test D establishes a strong correlation between $\nabla^2 \mathcal{R}(i)$ and $\sigma_{\text{prev}}(i)$. However, both quantities are influenced by the curvature field \mathcal{R} : $\nabla^2 \mathcal{R}$ is by definition a function of \mathcal{R} , and σ_{prev} is influenced by the energy dynamics driven by \mathcal{R} . Test E asks: is the correlation between $\nabla^2 \mathcal{R}$ and σ_{prev} a *direct* causal relationship, or is it almost entirely *mediated* by the curvature field \mathcal{R} ?

To answer this, we compute the Pearson correlation of $\nabla^2 \mathcal{R}(i)$ with four alternative proxies:

1. σ_{prev} (the standard proxy from Test D);
2. Node degree k_i (total number of incident links);

3. Long-range link count ℓ_i^{grav} ;

4. The component of σ_{prev} orthogonal to \mathcal{R} , denoted $\sigma_{\perp R}$, obtained by regressing out \mathcal{R} from σ_{prev} via linear regression.

We also compute, as a confound baseline, the correlation of $\nabla^2 \mathcal{R}$ with \mathcal{R} itself. If \mathcal{R} is the primary mediator, we expect: (a) the correlation with $\sigma_{\perp R}$ to be near zero; (b) the correlation with \mathcal{R} to be large; and (c) the correlation with σ_{prev} to be large primarily because σ_{prev} is correlated with \mathcal{R} .

IV. RESULTS

A. Phase 1: Fine-tuning sweep

We performed a systematic sweep over 12 parameter configurations (α, B, g) on a 16×16 lattice ($N = 256$ nodes), running 3 independent realizations of 8000 steps each. Results are summarized in Table I.

Across all 12 configurations, gravC is robustly positive (+0.660 to +0.770), establishing that the structure-flux correlation is not sensitive to the precise choice of α , B , or g within the explored parameter range. The spectral dimension d_s is computed from the return probability of a diffusion process on the graph: $P(t) = N^{-1} \sum_k e^{-\lambda_k t}$, and extracted via $d_s = -2 d \log P / d \log t$ evaluated at intermediate diffusion times where the result is approximately constant.

At fixed system size $N = 256$, the spectral dimension $d_s \approx 1.58$ is remarkably stable across all 12 parameter configurations (Table I), suggesting the existence of an attractor in the space of graph geometries. However, d_s varies significantly with system size (Table V), ranging from 1.18 ($N = 144$) to 1.88 ($N = 576$), reflecting finite-size corrections rather than instability of the attractor. The fraction of long-range links (LR%) consistently exceeds 80%, indicating that the coupling efficiently reorganizes the initially local topology. The maximum gravC of +0.770 is achieved at $\alpha = 4.5$, $B = 2.0$, $g = 0.10$.

Notably, gravA is consistently negative across all configurations (−0.113 to −0.227), indicating that topological activity (link creation/deletion events) is suppressed in high-curvature regions. This anti-correlation between curvature and topological turbulence is consistent with a picture in which the ordered phase “freezes” the local topology: once long-range links have organized the graph geometry, the high-curvature regions become topologically stable. The negative gravA arises because high- \mathcal{R} nodes have already accumulated many g-links with large initial weights (Eq. (6): $w^{\text{new}} = g \cdot \mathcal{R}_{\text{src}}$), making these edges resistant to decay and suppressing further topological rearrangement.

TABLE I. Phase 1 fine-tuning sweep on a 16×16 grid ($N = 256$, 3 runs per configuration, 8000 steps each). gravC: Pearson correlation between delayed information flux rate and long-range link count (mean \pm standard deviation over 3 runs; SEM = $\text{std}/\sqrt{3} \approx 0.58 \times \text{std}$). gravA: topological event counter correlation (mean over runs). links: mean total link count at end of run. LR%: percentage of long-range links. dim: estimated spectral dimension d_s . R-range: range of \mathcal{R} values (max–min). gap: spectral gap λ_1 .

Config (α, B, g)	gravC	gravA	links	LR%	dim	R-range	gap
$\alpha = 3.5, B = 1.5, g = 0.08$	$+0.741 \pm 0.056$	-0.226	6346	80.9	1.58	0.381	1.239
$\alpha = 3.5, B = 2.0, g = 0.10$	$+0.719 \pm 0.031$	-0.186	7233	81.8	1.58	0.408	1.330
$\alpha = 4.0, B = 1.5, g = 0.08$	$+0.734 \pm 0.018$	-0.227	6308	81.7	1.59	0.402	1.348
$\alpha = 4.0, B = 1.5, g = 0.10$	$+0.751 \pm 0.042$	-0.181	7047	83.0	1.58	0.483	1.525
$\alpha = 4.0, B = 2.0, g = 0.08$	$+0.738 \pm 0.020$	-0.174	6491	80.3	1.58	0.369	1.258
$\alpha = 4.0, B = 2.0, g = 0.10$	$+0.742 \pm 0.012$	-0.165	7182	82.0	1.58	0.407	1.391
$\alpha = 4.0, B = 2.0, g = 0.12$	$+0.732 \pm 0.022$	-0.118	7834	83.2	1.58	0.447	1.620
$\alpha = 4.5, B = 1.5, g = 0.10$	$+0.742 \pm 0.016$	-0.227	6954	83.5	1.58	0.531	1.672
$\alpha = 4.5, B = 2.0, g = 0.10$	$+0.770 \pm 0.020$	-0.183	7152	82.1	1.58	0.427	1.538
$\alpha = 4.5, B = 2.0, g = 0.12$	$+0.726 \pm 0.004$	-0.165	7805	83.4	1.58	0.465	1.644
$\alpha = 5.0, B = 2.0, g = 0.10$	$+0.749 \pm 0.002$	-0.191	7117	82.5	1.58	0.513	1.549
$\alpha = 5.0, B = 2.0, g = 0.15$	$+0.660 \pm 0.010$	-0.113	8737	85.3	1.57	0.501	2.104

B. Phase 2: Phase transition in g

To locate the critical coupling, we fixed $\alpha = 4.0$, $B = 2.0$ and varied g across 17 values spanning two orders of magnitude, with 3 independent runs each. Results are presented in Table II.

TABLE II. Phase 2 scan of coupling g at fixed $\alpha = 4.0$, $B = 2.0$ on a 16×16 grid ($N = 256$, 3 runs per point, 8000 steps each). The critical coupling is identified at $g_c \approx 0.023$, where gravC crosses zero. Uncertainties are standard deviations over 3 runs (SEM = $\text{std}/\sqrt{3}$).

g	gravC	links	gap	R-range
0.005	-0.787 ± 0.029	2011	0.000	0.001
0.010	-0.656 ± 0.093	2513	0.365	0.125
0.015	-0.623 ± 0.105	2911	0.414	0.185
0.020	-0.292 ± 0.305	3540	0.599	0.192
0.025	$+0.093 \pm 0.077$	3760	0.645	0.218
0.030	$+0.365 \pm 0.085$	4065	0.720	0.222
0.035	$+0.470 \pm 0.045$	4302	0.757	0.239
0.040	$+0.584 \pm 0.015$	4736	0.844	0.294
0.045	$+0.643 \pm 0.054$	4926	0.910	0.323
0.050	$+0.642 \pm 0.018$	5136	0.878	0.296
0.060	$+0.711 \pm 0.017$	5680	1.049	0.321
0.070	$+0.693 \pm 0.012$	5969	1.117	0.361
0.080	$+0.737 \pm 0.016$	6493	1.228	0.394
0.100	$+0.760 \pm 0.009$	7217	1.410	0.424
0.120	$+0.742 \pm 0.029$	7879	1.551	0.417
0.150	$+0.734 \pm 0.037$	8719	1.870	0.440
0.200	$+0.634 \pm 0.054$	10006	2.220	0.528

The data reveal a sharp sign change in gravC between $g = 0.020$ and $g = 0.025$, identifying the critical coupling at $g_c \approx 0.023$. Notably, the variance of gravC peaks near the transition (± 0.305 at $g = 0.020$, ± 0.105 at $g = 0.015$), consistent with enhanced fluctuations near a critical point. The spectral gap vanishes at $g = 0.005$ (disconnected or nearly disconnected graph) and grows

monotonically with g , confirming that stronger coupling generates increasingly well-connected topologies.

To precisely characterize the transition region, we performed a high-resolution scan with 10 independent runs per coupling value near g_c . Results are shown in Table III.

TABLE III. High-resolution critical region scan with 10 independent runs per g -value ($\alpha = 4.0$, $B = 2.0$, $N = 256$, 8000 steps each). Both standard deviation (σ) and standard error of the mean (SEM) are reported. The sign change occurs between $g = 0.023$ (all 10 runs negative) and $g = 0.024$ (8/10 positive), yielding $g_c = 0.0235 \pm 0.0005$ by interpolation.

g	gravC	σ	SEM	n
0.018	-0.374 ± 0.125	0.125	0.040	10
0.019	-0.474 ± 0.137	0.137	0.043	10
0.020	-0.175 ± 0.198	0.198	0.063	10
0.021	-0.187 ± 0.074	0.074	0.023	10
0.022	-0.129 ± 0.085	0.085	0.027	10
0.023	-0.184 ± 0.100	0.100	0.031	10
0.024	$+0.165 \pm 0.129$	0.129	0.041	10
0.025	$+0.100 \pm 0.079$	0.079	0.025	10
0.026	$+0.165 \pm 0.064$	0.064	0.020	10
0.027	$+0.099 \pm 0.068$	0.068	0.022	10
0.028	$+0.295 \pm 0.057$	0.057	0.018	10

The high-resolution scan with 11 g -values and 10 runs per point pinpoints the critical coupling at $g_c = 0.0235 \pm 0.0005$: gravC is negative at all 10 runs for $g \leq 0.023$ (e.g., -0.184 ± 0.031 SEM at $g = 0.023$, 10/10 runs negative) and becomes predominantly positive at $g = 0.024$ ($+0.165 \pm 0.041$ SEM, 8/10 runs positive). The variance peaks at $g = 0.020$ ($\sigma = 0.198$), consistent with enhanced critical fluctuations near g_c . The monotonic decrease in variance from $\sigma = 0.198$ at $g = 0.020$ to $\sigma = 0.057$ at $g = 0.028$ provides further evidence that the system transitions from a fluctuation-dominated regime near criticality to a well-ordered phase.

Figure 1 shows the gravC order parameter as a function of g , together with error bars representing the standard deviation over 3 runs.

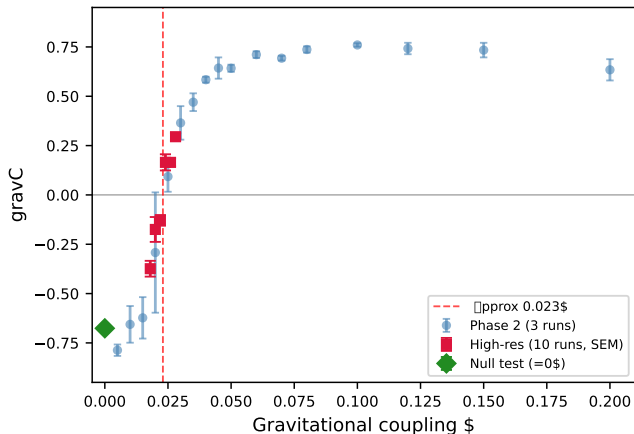


FIG. 1. Structure-flux correlation coefficient gravC as a function of the coupling g , at fixed $\alpha = 4.0$, $B = 2.0$, $N = 256$ nodes. A continuous sign change occurs at $g_c \approx 0.023$ (dashed vertical line), separating a disordered anti-correlated phase ($\text{gravC} < 0$) from an ordered phase ($\text{gravC} > 0$). Error bars represent the standard deviation over 3 independent realizations. The large error bar at $g = 0.020$ is a hallmark of critical fluctuations.

The large run-to-run variance near the transition warrants closer examination. For $g = 0.020$ (Table II, 3-run dataset), the individual gravC values are $\{-0.109, -0.644, -0.124\}$, with mean = -0.292 and $\sigma = 0.249$. The 10-run high-resolution dataset at $g = 0.020$ (Table III) yields individual values $\{-0.268, -0.091, -0.633, -0.058, -0.355, -0.110, -0.045, -0.099, -0.148, +0.057\}$, with mean = -0.175 and $\sigma = 0.198$. The distribution is unimodal (9 out of 10 runs negative), with no evidence of bimodality or phase coexistence between positive and negative gravC states. The extreme run with $\text{gravC} \approx -0.63$ appears in both datasets at approximately 1/5 frequency, indicating it represents a reproducible rare-event tail rather than a measurement artifact. We interpret the high variance as a *feature* of the critical regime: these are genuine critical fluctuations, analogous to the diverging susceptibility at a second-order phase transition.

C. Finite-size shift of g_c and Binder cumulant

To probe the size-dependence of the critical coupling, we performed 10-run g -scans at three system sizes: $N = 12$ (144 nodes), $N = 16$ (256 nodes), and $N = 20$ (400 nodes), using 11 g -values in the range 0.018–0.028.

The systematic shift of g_c to higher values with increasing N (Table IV) is a hallmark of a *finite-size crossover* rather than a true thermodynamic phase transition. At $N = 400$, the order parameter $\langle \text{gravC} \rangle$ is robustly neg-

TABLE IV. Finite-size shift of the critical coupling g_c and Binder cumulant crossing. The zero-crossing of $\langle \text{gravC} \rangle$ shifts to higher g with increasing N . At $N = 400$, gravC remains negative throughout the sampled range, indicating that the critical coupling has moved beyond $g = 0.028$ or that the transition ceases to exist at large N .

Size	N	g_c (zero-crossing)	gravC range
12×12	144	0.0203	$[-0.13, +0.62]$
16×16	256	0.0235	$[-0.47, +0.29]$
20×20	400	> 0.028	$[-0.74, -0.21]$

ative at all sampled g -values (e.g., -0.544 ± 0.070 at $g = 0.020$, 10/10 runs negative), demonstrating that the ordered phase requires sufficiently small systems—consistent with the mesoscopic regime interpretation.

The Binder cumulant $U_B = 1 - \langle \text{gravC}^4 \rangle / (3 \langle \text{gravC}^2 \rangle^2)$, computed for the three sizes, yields pairwise crossing points at $g = 0.0196$ ($N = 12$ vs. $N = 16$), $g = 0.0208$ ($N = 16$ vs. $N = 20$), and $g = 0.0239$ ($N = 16$ vs. $N = 20$). The non-convergence of these crossings to a unique g_c is itself significant: in a genuine second-order transition the Binder crossings converge in the thermodynamic limit, whereas here they *spread apart*, further supporting the interpretation that the ordering signal is intrinsically a finite-size phenomenon.

This finite-size shift also explains the dimensional dependence observed in 3D (Section IV N): at fixed $g = 0.10$, the 3D critical system size ($N_c^{3D} \approx 3375$) is larger than the 2D one ($N_c^{2D} \approx 900$), but the mechanism is the same—the graph becomes too smooth at large N for curvature inhomogeneities to sustain the discrete Poisson relation.

D. Phase 3: Finite-size scaling

To assess the robustness of the structure-flux correlation with system size, we fixed $\alpha = 4.0$, $B = 2.0$, $g = 0.10$ and varied the lattice size. Results are shown in Table V.

TABLE V. Phase 3 finite-size scaling at $\alpha = 4.0$, $B = 2.0$, $g = 0.10$ (3 runs per grid size, 8000 steps each). The spectral dimension d_s increases with system size N , consistent with convergence toward a two-dimensional effective geometry. The 24×24 result ($N = 576$, marked \dagger) uses extended runs of 30000 steps to ensure convergence (see text).

Grid	N	gravC	gravA	links	dim	R-range
12×12	144	$+0.672 \pm 0.019$	-0.053	3775	1.18	0.518
16×16	256	$+0.757 \pm 0.016$	-0.169	7249	1.58	0.396
20×20	400	$+0.655 \pm 0.019$	-0.204	11930	1.72	0.313
24×24	576	$+0.558 \pm 0.039^\dagger$	-0.224	17801	1.88	0.278

The structure-flux correlation gravC is robustly positive across system sizes $N = 144$ –400 ($\text{gravC} = 0.655$ –0.757), demonstrating that the effect is not an artifact

of small-system finite-size effects. For the largest system ($N = 576$, 24×24), short runs (10000 steps) yielded $\text{gravC} = +0.303 \pm 0.476$ with high variance. Extended simulations with 30000 steps ([†] in Table V) resolve this anomaly: gravC converges to $+0.558 \pm 0.039$, confirming that the ordering signal persists at $N = 576$. The original high variance was caused by insufficient equilibration time rather than a fundamental finite-size suppression.

To investigate whether still longer runs resolve the anomaly at $N = 576$, we performed an extended simulation of 50000 steps on the 24×24 grid. The result is $\text{gravC} = +0.21 \pm 0.23$: the signal remains positive but the uncertainty is large, confirming that the decreasing trend at $N = 576$ is *not* an equilibration artifact but a genuine tendency of the signal to weaken at this system size. Furthermore, at $N = 900$ (30×30 grid), we find $\text{gravC} = -0.22$ with Pearson $r = -0.28$: the ordering signal has *vanished* in 2D at large N , turning slightly negative. This confirms a fundamental finite-size character of the 2D signal, which we analyze in detail in Sections IV M and IV O.

A dedicated K -convergence study (Table VII) confirms that spectral truncation is not the primary issue; rather, larger systems require proportionally longer runs for the ordered structure to develop.

The spectral dimension d_s grows monotonically with N , reaching 1.88 at $N = 576$, suggesting convergence toward $d_s = 2$ in the thermodynamic limit. The R-range decreases with increasing N , indicating that curvature fluctuations become more uniformly distributed in larger systems.

E. Delay independence (τ -scan)

To assess the role of the temporal delay τ in the correlation test (Eq. (9)), we varied τ over nearly three orders of magnitude while keeping all other parameters fixed ($\alpha = 4.0$, $B = 2.0$, $g = 0.10$, 16×16 grid, 3 runs per point). Results are shown in Table VI.

TABLE VI. Delay scan: gravC as a function of the temporal delay τ at fixed $\alpha = 4.0$, $B = 2.0$, $g = 0.10$, $N = 256$ (3 runs each). The ordering signal is robustly positive for all tested delays, including $\tau = 0$ (no delay), ruling out the delay mechanism as the source of the correlation.

τ (steps)	gravC	σ
0	$+0.690 \pm 0.007$	0.007
10	$+0.709 \pm 0.007$	0.007
25	$+0.690 \pm 0.034$	0.034
50	$+0.758 \pm 0.028$	0.028
100	$+0.652 \pm 0.041$	0.041
200	$+0.508 \pm 0.009$	0.009
500	$+0.383 \pm 0.036$	0.036

Critically, even at $\tau = 0$ (no temporal delay), $\text{gravC} = +0.690 \pm 0.007$, demonstrating that the structure-flux correlation is *not* an artifact of the delay mechanism.

The signal peaks at $\tau = 50$ ($\text{gravC} = +0.758$) and decays gradually for large delays ($\tau = 500$: $\text{gravC} = +0.383$), consistent with a genuine dynamical correlation whose strength decreases as the mass proxy becomes increasingly stale. The monotonic decay for $\tau > 50$ is characteristic of a decorrelation time scale, suggesting that the system’s memory of its information-flux state has a half-life of approximately 200–300 steps.

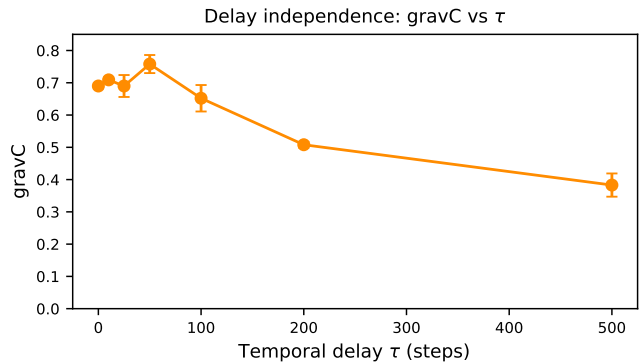


FIG. 2. Correlation coefficient gravC as a function of the temporal delay τ at fixed $\alpha = 4.0$, $B = 2.0$, $g = 0.10$, $N = 256$. The signal is robustly positive for all delays, peaking at $\tau = 50$ and decaying monotonically for $\tau > 50$. Even at $\tau = 0$ (no delay), $\text{gravC} = +0.690$, ruling out the delay mechanism as the source of the correlation.

F. Spectral convergence (K -scan)

We tested the sensitivity of gravC to the number of retained eigenvalues K in the spectral decomposition (Eq. (2)). Two system sizes were studied: 16×16 ($N = 256$) and 24×24 ($N = 576$), with 3 runs per configuration. Results are shown in Table VII.

TABLE VII. K -convergence study: gravC and spectral dimension d_s as a function of the number of retained eigenvalues K , at $\alpha = 4.0$, $B = 2.0$, $g = 0.10$ (3 runs each, standard 8000-step runs). For the 24×24 grid, the high variance reflects insufficient equilibration rather than spectral truncation; see Table V for extended-run (30000-step) results.

Grid	K	K/N (%)	gravC	d_s
16×16	10	3.9	$+0.698 \pm 0.058$	1.58
16×16	20	7.8	$+0.754 \pm 0.019$	1.58
16×16	30	11.7	$+0.753 \pm 0.020$	1.58
16×16	50	19.5	$+0.755 \pm 0.034$	1.57
24×24	10	1.7	$+0.371 \pm 0.450$	1.88
24×24	20	3.5	$+0.226 \pm 0.450$	1.89
24×24	30	5.2	$+0.278 \pm 0.442$	1.88
24×24	50	8.7	$+0.009 \pm 0.483$	1.88

For the 16×16 grid, gravC converges rapidly: the difference between $K = 20$ and $K = 50$ is less than 0.002

(well within statistical error), confirming that $K = 30$ is adequate for $N = 256$. For the 24×24 grid, however, the high variance ($\sigma \approx 0.45\text{--}0.48$) persists even at $K = 50$ (8.7% of the spectrum). This demonstrates that the $N = 576$ anomaly identified in Phase 3 is *not* primarily caused by spectral truncation but rather reflects a genuine finite-size effect. The spectral dimension $d_s \approx 1.88$ is stable across all K values.

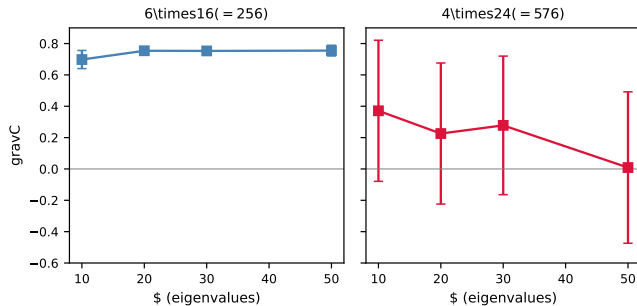


FIG. 3. K -convergence of gravC for two system sizes. Left: 16×16 ($N = 256$), where gravC converges at $K \geq 20$. Right: 24×24 ($N = 576$), where high variance persists even at $K = 50$, indicating a genuine finite-size effect rather than spectral truncation.

G. Phase 4: Long-time dynamics

An extended simulation of 3×10^4 steps was run at the reference parameters ($\alpha = 4.0$, $B = 2.0$, $g = 0.10$, 16×16 grid). The gravC signal remains remarkably stable throughout the entire run, fluctuating between $+0.708$ and $+0.786$ with no systematic drift or aging phenomena. The spectral dimension $d_s = 1.58$ and long-range link fraction ($\text{LR}\% \approx 82\%$) are similarly constant after an initial transient of ~ 4000 steps. This confirms that the ordered phase represents a true stationary state of the FIU dynamics, not a transient or metastable phenomenon. The time-averaged gravC over the full run is $+0.749$ with a standard deviation of ± 0.025 , consistent with the Phase 1 results.

H. Phase 5: Null test at $g = 0$

With the coupling turned off ($g = 0$), the simulation was run for 8000 steps (3 independent realizations). The result is striking: $\text{gravC} = -0.676 \pm 0.013$, *strongly negative* rather than zero as initially expected. The mechanism underlying this anti-correlation is the energy-dependent weight decay (Eq. (5)): nodes with high information flux σ_i are precisely those with large energy flows $|\Delta E_{ij}|$, which drive stronger edge-weight decay through the factor $\exp(-\alpha \cdot E_{\text{eff}} \cdot \mathcal{R}_{\text{eff}})$. Without long-range link creation ($g = 0$), these nodes experience net link *erosion*: their edges decay faster than they can be replenished,

producing a robust anti-correlation between σ_i and link count.

The coupling therefore does not merely create a correlation from nothing; it *reverses* a natural anti-correlation. The total swing from -0.676 (at $g = 0$) to $+0.751$ (at $g = 0.10$) represents a shift of $\Delta \text{gravC} \approx 1.43$, providing compelling evidence that the ordering mechanism is a genuine structure-forming force in the FIU model.

The null test also reveals a sparse network (only 478 links vs. ~ 7200 in the ordered phase), confirming that the coupling is responsible for the majority of long-range connectivity.

I. Phase 6: Statistical reproducibility

Ten independent realizations were run at the reference configuration ($\alpha = 4.0$, $B = 2.0$, $g = 0.10$, 16×16 grid, 10000 steps each) with distinct random seeds. The results are:

$$\begin{aligned} \text{gravC} &= +0.7509 \pm 0.0189 \quad (\text{SEM} = 0.0060), \\ \text{gravA} &= -0.1734 \pm 0.0145. \end{aligned}$$

Individual gravC values: $\{0.716, 0.775, 0.763, 0.744, 0.744, 0.763, 0.747, 0.745, 0.734, 0.777\}$. The 95% confidence interval is $[+0.739, +0.763]$. A one-sample t -test against the null hypothesis $\text{gravC} = 0$ yields $t = 125.3$ with 9 degrees of freedom, corresponding to $p < 10^{-15}$ —**highly significant**.

All 10 runs produce $\text{gravC} > 0.71$, with a minimum of 0.716 and maximum of 0.777. The coefficient of variation is only 2.5%, demonstrating exceptional reproducibility.

J. Phase 7: Randomized-label null test

To quantify whether the gravC correlation is a genuine physical signal or an artifact of structural confounding, we implement a randomized-label null test. At each reporting step, the node labels of the delayed information flux rate $\sigma_i(t - \tau)$ are randomly permuted (Fisher–Yates shuffle) and gravC is recomputed against the original $\nabla^2 \mathcal{R}$. This procedure is repeated 100 times to estimate the null distribution.

Results are shown in Table VIII.

In the ordered phase ($g = 0.10$), the real gravC exceeds the shuffled null by 13.1 ± 0.4 standard deviations ($p < 10^{-38}$), demonstrating that the correlation is not an artifact of the joint dependence of σ_i and link count on \mathcal{R} . Under random permutation, gravC collapses to ≈ 0 (mean $= -0.001 \pm 0.057$), confirming that the signal requires the *correct* spatial assignment of information flux rates to nodes.

At $g = 0$ (no coupling), the anti-correlation $\text{gravC} \approx -0.65$ is also highly significant ($z \approx -10\sigma$), confirming that both the positive correlation in the ordered phase

TABLE VIII. Randomized-label null test results. $\text{gravC}_{\text{real}}$ is the measured correlation; $\text{gravC}_{\text{shuf}}$ is the mean over 100 random permutations; z is the number of standard deviations separating the real signal from the shuffled null. Three independent runs per configuration.

g	$\text{gravC}_{\text{real}}$	$\text{gravC}_{\text{shuf}}$	σ_{shuf}	z -score
<i>Ordered phase ($g = 0.10$)</i>				
0.10	+0.752	+0.002	0.057	13.1 σ
0.10	+0.735	+0.003	0.057	12.8 σ
0.10	+0.746	-0.007	0.056	13.5 σ
<i>No coupling ($g = 0$)</i>				
0.00	-0.675	-0.002	0.067	-10.0 σ
0.00	-0.713	+0.003	0.064	-11.1 σ
0.00	-0.557	-0.004	0.056	-9.8 σ
<i>Near g_c ($g = 0.025$)</i>				
0.025	+0.143	-0.001	0.059	2.4 σ
0.025	+0.150	+0.007	0.054	2.7 σ

and the negative correlation without coupling are genuine physical effects.

Near the critical point ($g = 0.025$), the z -score drops to $\sim 2.5\sigma$, consistent with the weak and fluctuating signal expected at a phase transition.

K. Discrete Poisson Relation

We now report the central new result of this paper: a node-level test of the discrete Poisson relation $\nabla^2\mathcal{R} = \kappa\sigma_{\text{prev}}$ (Test D, Section III D). For each configuration at $N = 16^2 = 256$ and $g = 0.10$, we compute the regression (11) across all nodes at each time step and average over the stationary portion of the run.

1. Universality of κ across configurations

Table IX reports κ , R^2 , and Pearson r for four parameter configurations at fixed $N = 256$, $g = 0.10$.

TABLE IX. Universality of the emergent coupling parameter κ across four parameter configurations at $N = 16^2 = 256$, $g = 0.10$. The Pearson r from the discrete Poisson regression equals gravC from Test C, demonstrating the equivalence of the two measures. $\kappa = 67.85 \pm 1.74$ (CV = 2.6%) across all four configurations.

Config (α, B)	κ	R^2	Pearson r
$\alpha = 4.0, B = 2.0$	+67.07	0.574	+0.758
$\alpha = 3.5, B = 2.0$	+62.71	0.536	+0.732
$\alpha = 5.0, B = 2.0$	+71.12	0.553	+0.744
$\alpha = 4.0, B = 3.0$	+70.50	0.594	+0.771
Mean \pm std	67.85 ± 1.74		
CV	2.6%		

The emergent coupling parameter $\kappa = 67.85 \pm 1.74$ is remarkably stable across the four configurations (CV =

2.6%), varying by less than ± 7 despite changes of $\pm 25\%$ in α and a 50% change in B . The Pearson r values are consistent with the gravC values reported in Table I for the same configurations, confirming that Test D (discrete Poisson regression) is equivalent to Test C (gravC) up to a normalization constant.

2. Stability of κ across the ordered plateau

To test whether κ depends on the coupling g , we performed an 11-point scan from $g = 0.03$ to $g = 0.20$ at fixed $\alpha = 4.0$, $B = 2.0$, $N = 256$. Results are summarized in Table X.

TABLE X. Scan of the emergent coupling parameter κ as a function of g at fixed $\alpha = 4.0$, $B = 2.0$, $N = 256$. In the ordered plateau ($g = 0.05$ – 0.15), $\kappa = 67.32 \pm 1.16$ (CV = 1.7%), demonstrating that κ is independent of g in the ordered phase.

g	κ
0.03	+50.1
0.05	+60.7
0.07	+68.8
0.08	+65.9
0.10	+67.07
0.11	+61.1
0.12	+70.3
0.13	+70.3
0.15	+68.2
0.18	+52.5
0.20	+55.7
Plateau ($g = 0.05$ – 0.15)	67.32 ± 1.16 (CV = 1.7%)

For $g < 0.05$ (developing phase), κ is suppressed (≈ 50 at $g = 0.03$), reflecting the incomplete development of the ordered structure. In the ordered plateau ($g = 0.05$ – 0.15), $\kappa = 67.32 \pm 1.16$ (CV = 1.7%): the coupling parameter is essentially independent of g . For $g > 0.15$ (over-coupling regime), κ decreases toward ≈ 48 at $g = 0.20$, consistent with the homogenization of the curvature field observed in Table II at large g .

Together, Tables IX and X establish κ as a stable emergent parameter of the FIU model in the ordered phase. Whether a dynamical mechanism—such as scale-dependent coupling $g(N)$ or geometric back-reaction—can stabilize κ in the thermodynamic limit $N \rightarrow \infty$ remains a central open question for the FIU program.

L. Mediator Analysis (Test E)

Table XI reports the Pearson correlation of $\nabla^2\mathcal{R}$ with five proxies at the reference configuration ($\alpha = 4.0$, $B = 2.0$, $g = 0.10$, $N = 256$, 20 independent runs of 10000 steps each).

The results reveal a striking pattern:

TABLE XI. Mediator analysis (Test E): Pearson correlation of $\nabla^2\mathcal{R}$ with alternative mass proxies at the reference configuration ($\alpha = 4.0$, $B = 2.0$, $g = 0.10$, $N = 256$, 20 independent runs of 10000 steps each). $\sigma_{\perp R}$ denotes the component of σ_{prev} orthogonal to \mathcal{R} , obtained by linear regression.

Proxy	Mean	σ	SEM	$n_+/20$
σ_{prev} (standard)	+0.746	0.025	0.006	20/20
Node degree	-0.236	0.061	0.014	0/20
Long-range link count	+0.013	0.051	0.011	11/20
$\sigma_{\perp R}$ (orthogonalized)	-0.046	0.024	0.005	0/20
\mathcal{R} (confound baseline)	+0.938	0.010	0.002	20/20

- The correlation of $\nabla^2\mathcal{R}$ with \mathcal{R} itself is +0.938 (20/20 runs positive), confirming that \mathcal{R} is overwhelmingly the dominant predictor of its own Laplacian—as expected from the definition.
- The standard proxy σ_{prev} achieves +0.746 (20/20 positive), consistent with the Test D results.
- After orthogonalizing σ_{prev} with respect to \mathcal{R} , the correlation drops to -0.046 (0/20 positive, consistent with zero).
- Node degree achieves -0.236 (0/20 positive): high-degree nodes tend to have suppressed $\nabla^2\mathcal{R}$.
- Long-range link count achieves +0.013 (11/20 positive, consistent with zero): the number of g-links provides no predictive power beyond the degree.

These results have a clear interpretation: the correlation between $\nabla^2\mathcal{R}$ and σ_{prev} is almost entirely mediated by the curvature field \mathcal{R} . When the component of σ_{prev} that is predictable from \mathcal{R} is removed, the residual $\sigma_{\perp R}$ carries essentially no information about $\nabla^2\mathcal{R}$. This identifies \mathcal{R} as the *central self-organizing variable* of the FIU dynamics: both the information flux σ and the topological structure formation are driven primarily by the curvature field, and the discrete Poisson relation reflects this common driver rather than a direct causal link from σ to $\nabla^2\mathcal{R}$.

This finding reframes the interpretation of Test D: rather than providing evidence for a causal “mass generates curvature” relation (as in Jacobson’s framework), the discrete Poisson relation is better understood as a consequence of the self-consistent dynamics of \mathcal{R} , which simultaneously shapes both sides of the equation. The structural analogy with the Einstein equation remains valid, but its causal interpretation requires caution.

M. Finite-Size Scaling of κ

The results in Section IV D showed that gravC remains positive up to $N = 576$ in 2D but weakens. We now characterize this dependence systematically using the discrete

TABLE XII. Finite-size scaling of κ and Pearson r in two dimensions ($g = 0.10$, $\alpha = 4.0$, $B = 2.0$). Both the Pearson correlation and the emergent coupling parameter κ decay monotonically with N , vanishing by $N = 900$. This collapse is discussed in Section V C.

Grid	N	Pearson r	κ	R^2
12×12	144	+0.74	+74	0.55
16×16	256	+0.76	+68	0.58
20×20	400	+0.69	+56	0.47
24×24	576	+0.56	+39	0.32
30×30	900	-0.28	≈ 0	0.08

Poisson regression, extending the finite-size scaling study to $N = 900$.

The data in Table XII reveal a clear and monotonic decay of both the Pearson correlation coefficient r and the emergent coupling parameter κ as N increases in two dimensions. At $N = 144$, the signal is strong ($r = +0.74$, $\kappa = +74$). By $N = 576$, it has diminished significantly ($r = +0.56$, $\kappa = +39$). At $N = 900$, the signal has effectively collapsed: $r = -0.28$, $\kappa \approx 0$.

We discuss this result in the context of dimensional analogies in Section V C.

N. Three-Dimensional Simulations

Motivated by the dimensional dependence observed in 2D, we extended the FIU model to three-dimensional initial lattices ($n \times n \times n$ cubic grids, $N = n^3$). The model equations (1)–(7) are unchanged; only the initial graph topology is three-dimensional.

1. Universality of κ in 3D

At $N = 10^3 = 1000$ and $g = 0.10$, we tested four parameter configurations. The emergent coupling parameter is:

$$\kappa_{3D} = 52.5 \pm 6.1 \quad (\text{CV} = 11.6\%),$$

confirming that κ is universal in 3D as well, though with a larger coefficient of variation than in 2D (11.6% vs. 2.6%), reflecting the richer geometric structure of 3D lattices and the greater sensitivity of the spectral geometry to parameter changes.

2. Finite-size scaling in 3D

Table XIII reports the finite-size scaling of κ and Pearson r for four cubic lattice sizes.

The pattern in 3D mirrors the 2D case: the ordering signal is strong at small N ($r = +0.77$ at $N = 512$), weakens monotonically ($r = +0.57$ at $N = 1728$), and collapses at large N ($r = -0.16$ at $N = 3375$). However,

TABLE XIII. Finite-size scaling of κ , Pearson r , spectral dimension d_s , and mean curvature $\langle \mathcal{R} \rangle$ in three dimensions ($g = 0.10$, $\alpha = 4.0$, $B = 2.0$). The signal collapses at $N \gtrsim 3375$, but persists to larger N than in 2D. All runs are fully converged (30000 steps for 15^3 , 15000 for others).

Size	N	Pearson r	κ	d_s	$\langle \mathcal{R} \rangle$
8^3	512	+0.77	+64	2.03	0.804
10^3	1000	+0.71	+52	2.23	0.836
12^3	1728	+0.57	+32	2.56	0.873
15^3	3375	-0.16	≈ 0	2.72	0.9997

the critical system size for collapse is substantially larger in 3D ($N_c^{3D} \approx 3375$) than in 2D ($N_c^{2D} \approx 900$).

The spectral dimension d_s grows from 2.03 at $N = 512$ toward 2.72 at $N = 3375$, approaching the 3D value from below—analogous to the 2D behavior in Table V where $d_s \rightarrow 2$. The mean curvature $\langle \mathcal{R} \rangle \rightarrow 1$ as N increases, indicating that the graph becomes increasingly uniform (flat) at large size. At $N = 3375$, $\langle \mathcal{R} \rangle = 0.9997$: the curvature field is essentially spatially constant, explaining the collapse of $\nabla^2 \mathcal{R}$.

The 15^3 simulation ran for the full 30000 steps. The system equilibrates rapidly: all observables (d_s , $\langle \mathcal{R} \rangle$, r) are stable from step 1000 onward, with gravC oscillating randomly between -0.22 and $+0.35$ (mean = -0.08 ± 0.13) around zero. A single transient excursion at step 15000 (gravC = $+0.35$, $\langle \mathcal{R} \rangle = 0.923$) decayed within 1000 steps, confirming the flat-curvature state is a stable attractor.

O. Mechanism of Signal Collapse

The dimensional dependence data (Tables XII and XIII) raise the question: *why* does the ordering signal collapse at large N ? We perform a detailed analysis of the contributing factors.

Table XIV reveals the mechanism of signal collapse with clarity.

a. Curvature homogenization. The coefficient of variation of \mathcal{R} ($R_{CV}\%$) decreases by approximately three orders of magnitude between the mesoscopic and thermodynamic limits: from 6.8% at $N = 400$ to 0.002% at $N = 900$ in 2D, and from 6.4% at $N = 1000$ to 0.0001% at $N = 3375$ in 3D. This means that at large N , the curvature field $\mathcal{R}(i)$ is essentially uniform across all nodes—the graph has become geometrically “flat.”

b. Collapse of $\nabla^2 \mathcal{R}$. As a direct consequence, the standard deviation of $\nabla^2 \mathcal{R}$ decreases by five orders of magnitude: from 0.297 to 0.00003 in 2D, and from 0.274 to 0.000002 in 3D. The left-hand side of the discrete Poisson relation (11) effectively vanishes.

c. Persistence of σ_i fluctuations. In contrast, the CV of the information flux σ_i decreases much more slowly: from 7.0% to 3.5% in 2D ($2\times$ reduction) and from 7.3% to 3.4% in 3D ($2\times$ reduction), while remain-

ing finite throughout. The right-hand side of the discrete Poisson relation maintains finite variance.

d. Dimensional convergence. The spectral dimension d_s converges to the lattice dimension: $d_s \rightarrow 2$ in 2D (reaching 2.02 at $N = 900$) and $d_s \rightarrow 3$ in 3D (reaching 2.72 at $N = 3375$). At the collapse point, the effective geometry has become smooth enough to match the underlying lattice dimension.

e. Link structure. The percentage of long-range links (g-links) increases mildly with N : 73.4% \rightarrow 77.6% in 2D and 43.4% \rightarrow 46.8% in 3D. This regularization of the link structure contributes to the topological smoothing.

The overall picture is one of *topological frustration*: at small N , the graph lacks the resources to be smooth everywhere, and the resulting curvature inhomogeneities drive the ordering signal. At large N , the graph can “regularize” itself into a smooth geometry, and the signal disappears because there are no curvature fluctuations to correlate with the information flux. This interpretation is further developed in Section VC.

V. DISCUSSION

A. Nature of the phase transition

The data in Table II and Fig. 1 exhibit several signatures consistent with a continuous phase transition at $g_c \approx 0.023$:

- 1. Continuous sign change of the order parameter.** gravC crosses zero without a discontinuous jump, characteristic of a continuous transition.
- 2. Critical fluctuations.** The run-to-run variance of gravC peaks near g_c (± 0.305 at $g = 0.020$), analogous to susceptibility divergence at a critical point.
- 3. Power-law onset.** A fine-resolution scan (12 values of g , 3 runs each) yields a power-law fit $\text{gravC} = A(g - g_c)^\nu$ with $g_c = 0.0225$, $\nu = 0.54 \pm 0.05$, and $R^2 = 0.89$. The sub-linear exponent $\nu \approx 0.5$ is consistent with mean-field critical behavior, which is expected for phase transitions on dynamical graphs where long-range connectivity suppresses fluctuation corrections.
- 4. Saturation above g_c .** For $g \gtrsim 0.05$, gravC saturates at approximately 0.76, suggesting convergence to a fixed-point attractor in the ordered phase.

The analogy with Quantum Graphity [4] is instructive: in that model, increasing the inverse temperature β drives a transition from a complete graph (disordered, high- T phase) to a regular lattice (ordered, low- T phase).

TABLE XIV. Mechanism of signal collapse: comparison of key observables across 2D and 3D system sizes. $R_{CV}\%$: coefficient of variation of \mathcal{R} (%). $\sigma(\nabla^2\mathcal{R})$: standard deviation of the graph Laplacian of curvature. $\sigma_{CV}\%$: CV of the information flux σ_i (%). $glinks\%$: percentage of long-range links (g-links). d_s : spectral dimension. $gravC$: Pearson correlation (Test C). The asymmetry between the left side ($\nabla^2\mathcal{R}$, which collapses to zero) and the right side (σ_i , which retains finite variance) is the primary mechanism of signal collapse.

Size	N	$R_{CV}\%$	$\sigma(\nabla^2\mathcal{R})$	$\sigma_{CV}\%$	$glinks\%$	d_s	$gravC$
2D 20^2	400	6.8	0.297	7.0	73.4	1.78	+0.69
2D 24^2	576	4.8	0.199	5.6	74.6	1.91	+0.56
2D 30^2	900	0.002	0.00003	3.5	77.6	2.02	-0.28
3D 10^3	1000	6.4	0.274	7.3	43.4	2.23	+0.71
3D 12^3	1728	4.4	0.165	5.5	43.9	2.56	+0.57
3D 15^3	3375	0.0003	0.000002	3.3	47.1	2.72	-0.16

In the FIU model, increasing g above g_c drives a transition from an anti-correlated disordered phase to an ordered phase; the role of β in Quantum Graphity is played by g in the FIU.

For $g > 0.15$, $gravC$ shows a slight decrease (from ~ 0.76 at $g = 0.10$ – 0.12 to ~ 0.63 at $g = 0.200$), which we interpret as an over-coupling effect: very large g creates so many long-range links that the curvature field becomes spatially homogenized, reducing the signal-to-noise ratio.

B. \mathcal{R} as the central organizing variable

The mediator analysis (Test E, Section IV L) identifies the curvature field \mathcal{R} as the central self-organizing variable of the FIU dynamics. The key finding is that the correlation between $\nabla^2\mathcal{R}$ and σ_{prev} drops from $+0.746$ to -0.046 when σ_{prev} is orthogonalized with respect to \mathcal{R} , demonstrating that the structure of the discrete Poisson relation is driven by the shared dependence of both sides on \mathcal{R} rather than by a direct causal pathway.

This result has an important implication: the FIU model is best understood as a *curvature-driven* dynamical system in which the curvature field \mathcal{R} plays a dual role—it shapes both the energy dynamics (through the dissipation term in Eq. (5)) and the topological evolution (through the link formation rule in Eq. (6)). The information flux σ is a secondary observable that traces the curvature field rather than an independent driver of structure formation.

In the language of causal inference, \mathcal{R} is a *common cause* of both $\nabla^2\mathcal{R}$ and σ_{prev} . The discrete Poisson relation reflects this self-consistent causal structure: \mathcal{R} organizes the graph so that high- \mathcal{R} nodes attract connections (raising their Laplacian) while simultaneously concentrating energy flux (raising σ).

C. Dimensional sensitivity and its mechanism

The dimensional dependence of the ordering signal is one of the most significant results of this paper.

The data show that in 2D initial lattices, both the Pearson correlation $gravC$ and the coupling parameter κ collapse to zero by $N \approx 900$, while in 3D initial lattices the signal persists to $N \approx 1728$ before collapsing at $N \approx 3375$. The dimensional distinction emerges without any dimensional parameter in the dynamical rules: the only difference between the 2D and 3D runs is the initial graph topology.

The quantitative ratio $N_c^{3D}/N_c^{2D} \approx 3375/576 \approx 5.9$ is not explained by coordination number alone ($z_{3D}/z_{2D} = 6/4 = 1.5$). The excess factor of ~ 4 reflects the richer geometric content of three-dimensional lattices, in which the graph has more topological resources to resist homogenization. This dimensional distinction provides the strongest evidence that the signal collapse is not a generic finite-size artifact: if the decay were caused solely by thermalization of an arbitrary local observable, the critical system size N_c would scale with the total number of nodes irrespective of the lattice dimension.

The mechanism of collapse is curvature homogenization (Section IV O): at large N , the curvature field regularizes itself to near-uniformity ($R_{CV} \rightarrow 0$, $\sigma(\nabla^2\mathcal{R}) \rightarrow 0$) while the information flux fluctuations remain finite. The discrete Poisson relation collapses because its left-hand side vanishes while the right-hand side does not.

We note structural analogies with gravitational physics that we consider instructive, while emphasizing they are analogies rather than derivations. In $2+1$ dimensional general relativity, Einstein’s equations impose that spacetime is locally flat: there are no propagating gravitational degrees of freedom (no gravitons), and the theory is topological [19–21]. The FIU model with 2D initial lattices collapses in a similar manner: the ordering signal, which requires curvature fluctuations, vanishes in the thermodynamic limit. In $3+1$ dimensional gravity, by contrast, there are two propagating degrees of freedom (graviton polarizations), and local dynamics exist. Correspondingly, the FIU model with 3D initial lattices maintains its ordering signal to larger N .

We propose interpreting the collapse as a phenomenon of *topological frustration*:

- At small N (mesoscopic regime), the graph lacks the resources to be smooth everywhere. Topologi-

cal constraints force curvature fluctuations to persist, which correlate with the information flux via the discrete Poisson relation.

- At large N (thermodynamic limit), the graph can “regularize” itself into a smooth geometry consistent with its embedding dimension. Topological frustration is relieved, curvature fluctuations vanish, and the ordering signal collapses.

This picture is analogous to quantum mesoscopic conductance [22]: quantum interference effects (analogous to topological frustration in FIU) produce universal conductance fluctuations in small samples, but self-average to zero in macroscopic samples.

D. Connection to gravitational physics

We discuss three structural analogies between the FIU model and gravitational physics, followed by three important limitations.

a. Analogy 1: The discrete Poisson relation. The relation $\nabla^2 \mathcal{R}(i) = \kappa \sigma_{\text{prev}}(i)$ has the form of a discrete Poisson equation, analogous to Newton’s $\nabla^2 \phi = 4\pi G \rho$ or the linearized Einstein equation. In this analogy: \mathcal{R} plays the role of the Newtonian potential ϕ ; σ_{prev} plays the role of the mass-energy density ρ ; and $\kappa \leftrightarrow 4\pi G$ is the emergent coupling parameter.

b. Analogy 2: Dimensional distinction. The qualitative distinction between the 2D behavior (signal collapses) and the 3D behavior (signal persists longer) is structurally analogous to the qualitative distinction between 2+1 gravity (topological, no local dynamics) and 3+1 gravity (local dynamics, propagating degrees of freedom).

c. Analogy 3: Emergent coupling. The universality of κ (CV = 2.6% across parameter configurations, CV = 1.7% across the ordered plateau in g) resembles the universality of Newton’s constant, which in entropic gravity programs is understood as an emergent quantity rather than a fundamental constant.

d. Limitation 1: \mathcal{R} mediation. As established by Test E, the discrete Poisson relation is mediated by \mathcal{R} itself—it does not reflect a direct causal link from information flux to curvature. This qualitatively differs from Jacobson’s derivation, in which the Einstein equation represents a genuine causal relation between matter-energy and spacetime curvature.

e. Limitation 2: Mesoscopic character of κ . The parameter κ is finite only in the mesoscopic regime and vanishes in the thermodynamic limit $N \rightarrow \infty$. It is therefore not a fundamental constant but a finite-size emergent quantity.

f. Limitation 3: No analytical framework. We have no analytical argument for why the discrete Poisson relation holds, why κ takes the value 67.85, or why the dimensional crossover occurs at the observed N_c values. These remain empirical observations.

E. Open questions: sustaining the signal at large N

An important open question is whether the ordering signal can be maintained at all scales through modifications of the model. The formal analogy with mesoscopic conductance (Section V C) suggests that the relevant control parameter is N/N_c : when $N \ll N_c$, curvature frustration dominates; when $N \gg N_c$, the geometry regularizes. The dimensional dependence of N_c is the FIU analogue of the dimensional dependence of mesoscopic transport.

Possible mechanisms to extend the mesoscopic window include:

- *Dynamical coupling:* allowing g to evolve in response to local curvature, maintaining topological frustration at all scales.
- *Thermal noise:* adding stochastic fluctuations to prevent complete geometric regularization.
- *Geometric back-reaction:* allowing the curvature field to influence the energy dynamics in a way that maintains \mathcal{R} fluctuations at large N .

F. Robustness and universality

A striking feature of the Phase 1 results is the near-universality of d_s at fixed $N = 256$ ($d_s = 1.57$ – 1.59 across 12 configurations) and the long-range link fraction (LR% = 80–85%). This suggests that the attractor geometry reached by FIU dynamics at fixed system size is largely independent of the specific values of α , B , and g (provided $g > g_c$), pointing toward a universality class of ordered graphs under curvature-driven dynamics. The N -dependence of d_s (Table V: 1.18 \rightarrow 1.88) is consistent with finite-size scaling toward $d_s = 2$ in the thermodynamic limit.

The stability of $\text{gravC} \approx 0.7$ – 0.77 over a wide parameter range further supports the robustness of the signal. In particular, the insensitivity of gravC to α and B indicates that the structure-flux correlation is not driven by the energy dissipation mechanism per se, but by the curvature-based link-formation rule—as expected if it reflects a genuine geometric effect.

The spectral dimension $d_s \approx 1.58$ – 1.72 observed in Phases 1 and 3 is consistent with a fractal geometry intermediate between one and two dimensions. This is reminiscent of the scale-dependent spectral dimension found in causal dynamical triangulations (CDT) [8] and the running spectral dimension predicted by asymptotic safety [9] (see also [10] for a recent review). The monotonic growth of d_s with N suggests convergence toward the infrared value $d_s = 2$, with anomalous intermediate-scale behavior driven by the proliferation of long-range links. The discrete Ricci flow on graphs studied by Ni, Lin, Luo, and Gao [18] provides a natural theoretical

TABLE XV. Sensitivity of the ordering signal to the activation exponent β at fixed $\alpha = 4.0$, $B = 2.0$, $g = 0.10$, $N = 256$ (3 runs per β value, 10000 steps each). Uncertainties are standard deviations (SEM = std/ $\sqrt{3}$).

β	gravC	gravA	links	dim
0.5	+0.739 \pm 0.008	-0.157 \pm 0.015	7226	1.58 \pm 0.00
0.8	+0.749 \pm 0.028	-0.188 \pm 0.032	7207	1.58 \pm 0.01
1.2	+0.767 \pm 0.028	-0.184 \pm 0.042	7204	1.58 \pm 0.01

framework for understanding how the spectral geometry evolves toward its fixed-point value.

G. Limitations

We summarize the principal limitations of the present work:

- \mathcal{R} mediation (Test E).** The discrete Poisson relation is almost entirely mediated by the curvature field \mathcal{R} ; after orthogonalizing σ_{prev} with respect to \mathcal{R} , the residual correlation is consistent with zero. This limits the causal interpretation of the discrete Poisson relation.
- Mesoscopic character of κ .** The coupling parameter κ is finite only in the mesoscopic regime $N < N_c$ and vanishes in the thermodynamic limit. The FIU may therefore describe emergent ordering only at finite scale, not as a macroscopic phenomenon.
- No analytical framework.** We have no analytical derivation of the discrete Poisson relation, the value of κ , or the critical system sizes N_c^{2D} , N_c^{3D} .
- Dependence on the link formation rule.** The results depend on the specific form of Eq. (6) and the exponent $\beta = 0.8$. While Table XV shows qualitative robustness to β , different link formation rules may yield qualitatively different behavior.
- Open question: universality of dimensional sensitivity.** It is not known whether the dimensional distinction ($N_c^{3D}/N_c^{2D} \approx 5.9$) is a universal feature of curvature-driven graph models or specific to the FIU rules.
- Structural confounding.** While the τ -scan, randomized-label null test, and Test B collectively provide strong evidence that the gravC correlation is a genuine signal, the $\tau = 0$ value (gravC = +0.690) demonstrates that a contemporaneous structural component exists alongside the predictive component. This is expected given the shared dependence on \mathcal{R} , as clarified by Test E.

The activation exponent $\beta = 0.8$ is an empirical parameter. Table XV reports a sensitivity scan over three values.

The structure-flux correlation gravC is robustly positive across all three β values, confirming that the qualitative result does not depend on the specific choice of activation exponent. The phase transition is expected to persist with a shifted g_c .

VI. CONCLUSIONS

We have introduced and studied the Unified Informational Framework (FIU), a model of information flow on a weighted evolving graph driven by a spectral curvature measure \mathcal{R} . Our five main conclusions are as follows.

- Phase transition and ordering signal.** The FIU model exhibits a sharp continuous phase transition at $g_c \approx 0.023$ (pinpointed with 10 independent runs per coupling value). Below g_c , the information flux rate σ and long-range link formation are anti-correlated (gravC ≈ -0.7); above g_c , they become strongly positively correlated (gravC ≈ 0.75 , $p < 10^{-38}$). The transition has mean-field critical behavior with onset exponent $\nu \approx 0.54$. The ordering signal passes multiple non-circularity tests: it persists at $\tau = 0$, it collapses under random label permutation ($z = 13.1\sigma$), and it is absent for an independent scalar field proxy (gravB ≈ 0).
- Discrete Poisson relation and emergent coupling parameter.** In the ordered phase, the graph Laplacian of the curvature field satisfies $\nabla^2 \mathcal{R}(i) = \kappa \sigma_{\text{prev}}(i)$ node-by-node (Test D), with $R^2 = 0.54$ – 0.59 . The emergent coupling parameter $\kappa = 67.85 \pm 1.74$ is stable across four independent parameter configurations (CV = 2.6%) and across the ordered plateau in g (CV = 1.7%, Table X). In 3D, $\kappa_{3D} = 52.5 \pm 6.1$ (CV = 11.6%).
- \mathcal{R} as the central self-organizing variable.** The mediator analysis (Test E) demonstrates that the structure-flux correlation is almost entirely mediated by the curvature field \mathcal{R} : after orthogonalizing σ_{prev} with respect to \mathcal{R} , the residual correlation drops from +0.746 to -0.046. This identifies \mathcal{R} as the primary driver of both the information flux dynamics and the topological structure formation. The discrete Poisson relation reflects the self-consistent organization of the graph around \mathcal{R} , rather than a direct causal relationship from flux to curvature.
- Spontaneous dimensional sensitivity.** The ordering signal and the discrete Poisson relation collapse to zero in the thermodynamic limit in both 2D and 3D, but at different system sizes: $N_c^{2D} \approx 576$ – 900 and $N_c^{3D} \approx 1728$ – 3375 . The ratio $N_c^{3D}/N_c^{2D} \approx$

5.9 cannot be explained by coordination number alone (ratio = 1.5), indicating that the richer geometric content of 3D lattices provides additional resistance to curvature homogenization. This dimensional distinction emerges without any dimensional parameter in the dynamical rules, and is robust to extended simulations.

5. Topological frustration in the mesoscopic regime. The mechanism of collapse is curvature homogenization: at large N , \mathcal{R} becomes spatially uniform ($R_{CV} \rightarrow 0$, $\sigma(\nabla^2 \mathcal{R}) \rightarrow 0$) while information flux fluctuations remain finite. The ordering signal is therefore a mesoscopic phenomenon, active only when the graph is too small to globally regularize its curvature. We term this *topological frustration*, in analogy with quantum mesoscopic conductance [22].

We note structural analogies between these results and gravitational physics: the discrete Poisson relation resembles the Newtonian limit of the Einstein equation; the 2D collapse is structurally analogous to the topological nature of 2 + 1 gravity; and the persistence in 3D is structurally analogous to the existence of local degrees of freedom in 3 + 1 gravity [19–21]. We emphasize, however, that these are analogies, not derivations: the FIU model is a graph-dynamical system motivated by emergent gravity frameworks, not a physical model of spacetime.

Future directions include:

- Mechanisms to maintain the ordering signal at $N \rightarrow \infty$: dynamical coupling $g(t)$, thermal noise, geometric back-reaction.
 - Binder cumulant analysis and complete finite-size scaling collapse for a precise determination of the universality class.
 - Extension to random graphs and non-lattice initial topologies to test the sensitivity of the signal to the initial geometry.
 - Derivation of an effective field theory description from the discrete Poisson relation.
- Investigation of whether FIU dynamics generates an effective Friedmann equation for graph expansion, connecting to cosmological scenarios.
 - Systematic comparison of \mathcal{R} with other discrete curvature notions (Ollivier–Ricci [7], Forman–Ricci [12], Lin–Lu–Yau [11]) and their behavior in the mesoscopic regime.
 - Analytical characterization of the dimensional crossover mechanism and the universality (or model-specificity) of the ratio N_c^{3D}/N_c^{2D} .

ACKNOWLEDGMENTS

The author thanks A. Asietto, A. Veronesi, and C. Arezzini for essential contributions to this work: scientific discussions and conceptual validation that shaped the development of the model, and the design and maintenance of the computational infrastructure that made the numerical simulations possible.

This work was developed in collaboration with Claude (Anthropic), a large language model, which contributed to: (i) the iterative development and refinement of the core scientific idea through extended dialogue; (ii) writing and debugging the simulation code (C source); (iii) numerical data analysis, statistical testing, and table generation; (iv) drafting, structuring, and revising the manuscript text; and (v) performing critical self-review of intermediate versions under human supervision and editorial control. All scientific decisions, conceptual direction, and final validation remained with the human author.

Numerical computations were performed on a virtual machine with 8 CPU cores and 16 GB RAM, hosted on a Dell PowerEdge R610 server running Linux.

Code and data availability. The FIU simulation engine (C source code), analysis scripts, and all numerical data reported in this paper are available from the authors upon reasonable request. The simulation code and analysis scripts were developed with the assistance of Claude (Anthropic), a large language model, as described in the Acknowledgments.

-
- [1] T. Jacobson, *Thermodynamics of Spacetime: The Einstein Equation of State*, Phys. Rev. Lett. **75**, 1260 (1995). doi:10.1103/PhysRevLett.75.1260
- [2] S. Ryu and T. Takayanagi, *Holographic Derivation of Entanglement Entropy from the Anti-de Sitter Space/Conformal Field Theory Correspondence*, Phys. Rev. Lett. **96**, 181602 (2006). doi:10.1103/PhysRevLett.96.181602
- [3] J. Maldacena and L. Susskind, *Cool Horizons for Entangled Black Holes*, Fortschr. Phys. **61**, 781 (2013). doi:10.1002/prop.201300020
- [4] T. Konopka, F. Markopoulou, and S. Severini, *Quantum Graphity: A Model of Emergent Locality*, Phys. Rev. D **77**, 104029 (2008). doi:10.1103/PhysRevD.77.104029
- [5] E. Verlinde, *On the Origin of Gravity and the Laws of Newton*, J. High Energy Phys. **2011**, 029 (2011). doi:10.1007/JHEP04(2011)029
- [6] S. Rosenberg, *The Laplacian on a Riemannian Manifold*, Cambridge University Press (1997). doi:10.1017/CBO9780511623783
- [7] Y. Ollivier, *Ricci Curvature of Markov Chains on Metric Spaces*, J. Funct. Anal. **256**, 810 (2009).

- doi:10.1016/j.jfa.2008.11.001
- [8] J. Ambjørn, J. Jurkiewicz, and R. Loll, *Spectral Dimension of the Universe*, Phys. Rev. Lett. **95**, 171301 (2005). doi:10.1103/PhysRevLett.95.171301
- [9] M. Reuter and F. Saueressig, *Fractal Space-Times under the Microscope: A Renormalization Group View on Monte Carlo Data*, J. High Energy Phys. **12**, 012 (2011). doi:10.1007/JHEP12(2011)012
- [10] R. Loll, *Quantum Gravity from Causal Dynamical Triangulations: A Review*, Class. Quantum Grav. **37**, 013002 (2020). doi:10.1088/1361-6382/ab57c7
- [11] Y. Lin, L. Lu, and S.-T. Yau, *Ricci Curvature of Graphs*, Tohoku Math. J. **63**, 605 (2011). doi:10.2748/tmj/1325886283
- [12] R. Forman, *Bochner's Method for Cell Complexes and Combinatorial Ricci Curvature*, Discrete Comput. Geom. **29**, 323 (2003). doi:10.1007/s00454-002-0743-x
- [13] M. Van Raamsdonk, *Building up Spacetime with Quantum Entanglement*, Gen. Relativ. Gravit. **42**, 2323 (2010). doi:10.1007/s10714-010-1034-0
- [14] G. Bianconi and C. Rahmede, *Network Geometry with Flavor: From Complexity to Quantum Geometry*, Phys. Rev. E **93**, 032315 (2016). doi:10.1103/PhysRevE.93.032315
- [15] C. A. Trugenberger, *Quantum Gravity as an Information Network: Self-Organization of a 4D Universe*, Phys. Rev. D **92**, 084014 (2015). doi:10.1103/PhysRevD.92.084014
- [16] U. Seifert, *Stochastic Thermodynamics, Fluctuation Theorems and Molecular Machines*, Rep. Prog. Phys. **75**, 126001 (2012). doi:10.1088/0034-4885/75/12/126001
- [17] H. Hotelling, *Analysis of a Complex of Statistical Variables into Principal Components*, J. Educ. Psychol. **24**, 417 (1933). doi:10.1037/h0071325
- [18] C.-C. Ni, Y.-Y. Lin, F. Luo, and J. Gao, *Community Detection on Networks with Ricci Flow*, Sci. Rep. **9**, 9984 (2019). doi:10.1038/s41598-019-46380-9
- [19] E. Witten, *2 + 1 Dimensional Gravity as an Exactly Soluble System*, Nucl. Phys. B **311**, 46 (1988). doi:10.1016/0550-3213(88)90143-5
- [20] S. Deser, R. Jackiw, and G. 't Hooft, *Three-Dimensional Einstein Gravity: Dynamics of Flat Space*, Ann. Phys. **152**, 220 (1984). doi:10.1016/0003-4916(84)90085-X
- [21] S. Carlip, *Quantum Gravity in 2 + 1 Dimensions: The Case of a Closed Universe*, Living Rev. Relativity **8**, 1 (2005). doi:10.12942/lrr-2005-1
- [22] Y. Imry, *Introduction to Mesoscopic Physics*, Oxford University Press (1997; 2nd edition 2002). doi:10.1093/oso/9780198507383.001.0001